Study on the *in vitro* and *in vivo* activation of rat hepatic stellate cells by Raman spectroscopy

Aiguo Shen*
Wuhan University
Institute of Analytical Biomedicine
Wuhan 430072, China
and
Wuhan University
School of Basic Medicine
Wuhan 430071, China

Zhangxiu Liao*
Hui Wang
Wuhan University
School of Basic Medicine
Wuhan 430071, China

Iiho Goan
Wuhan University
Institute of Analytical Biomedicine
Wuhan 430072, China

Yong Wu
Wuhan University
School of Basic Medicine
Wuhan 430071, China

Xiaohua Wang
Zhenyu Yu
Jiming Hu
Wuhan University
Institute of Analytical Biomedicine
Wuhan 430072, China

Abstract. The feasibility of a novel and efficient diagnostic method for liver fibrosis using Raman spectroscopy is studied. Confocal Raman spectroscopy (CRS) is utilized to monitor the molecular changes of hepatic stellate cells (HSCs) *in vitro* as well as *in vivo* activation. *In vitro* activation was induced by growth in uncoated plastic plates, while the *in vivo* activation is induced by a single intraperitoneal injection of carbon tetrachloride (CCl_4). The biochemical changes of HSCs during activation such as the loss of retinoid, the increase of α-helical protein, and the increased production of extracellular matrix proteins are observed by CRS. A user-friendly autoclassifying system is also developed to classify Raman spectra of liver injury tissues with a 90% accuracy rate. Raman spectroscopy combined with a fiber optical probe could be potentially accomplished for *in vivo* detection, which can lead to a novel and efficient diagnosis for liver fibrosis.
 [DOI: 10.1117/1.2749507]

Keywords: hepatic stellate cells; *in vivo*/*in vitro* activation; biochemical changes; Raman spectroscopy.

Paper 06203RR received Jul. 31, 2006; revised manuscript received Jan. 31, 2007; accepted for publication Feb. 20, 2007; published online Jun. 29, 2007.

1 Introduction

Hepatic stellate cells (HSCs; Ito cells[1]), comprising 5 to 8% of the total number of resident liver cells, play an important role in the pathogenesis of liver disease. The activation of HSCs represents a final common pathway of the hepatic response to liver injury.[2] Following an acute/chronic liver injury, the normally quiescent HSCs undergo a progressive activation or transdifferentiation into proliferative, fibrogenic, proinflammatory, and contractile myofibroblasts.[3] Since the activation of HSCs could be regarded as an early symbol of the hepatic fibrosis,[4] it was desirable to find a single, rapid, and precise technique to identify HSCs in the quiescent phenotype and after their activation.

Several methods for HSC phenotype identification such as fluorescence microscope,[4] flow cytometry,[5] Western blot analysis,[6] and immunochemistry,[7] have been reported. However, most of these methods are invasive and require complex preparation steps such as cell fixation, staining, protein extractions, etc. Hence there is a need to develop a suitable technique capable of directly characterizing HSC *in vivo* or *in vitro* activation.[4]

Raman spectroscopy is a well-established analytical tool and is based on the interaction of electromagnetic radiation with the molecules in the sample. The Raman spectrum provides useful information for chemical fingerprinting of the samples. This technique has three main advantages over conventional biological assays for the study of cells or tissues (1) it is rapid[8,9] (1 to 3 min), (2) it is noninvasive and no labels are required, and (3) no damage is induced to the biomedical samples if suitable laser wavelength and laser power are used.[9,10] It has been applied in the investigation of biomedical issues including quantitative histochemical analysis of human arteries,[11] disease diagnosis especially for cancer,[12,13] characterization of pterygium and normal bulbar conjunctiva,[14] imaging of cells,[15] and analysis of the stratum corneum in human skin in relation to administration of therapeutic agents.[16]

*A. G. Shen and Z. X. Liao contributed equally to this work.
Address all correspondence to Jiming Hu, Institute of Analytical Biomedicine, Wuhan University, Wuhan, Hubei 430072, China; Tel: +86–027–87882136; Fax: +86–027–87882136; E-mail: jmhu@whu.edu.cn

1083-3668/2007/12(3)/034003/9/$25.00 © 2007 SPIE

A few studies have been carried out on the application of Raman spectroscopy in hepatology. Hawi et al. used Raman microspectroscopy to characterize normal and malignant hepatocytes in cultured cells and in human liver tissues.[17] In this study, we successfully isolated HSCs and induced cell *in vitro* activation using growth in uncoated plastic plates and *in vivo* activation by a single intraperitoneal injection of CCl_4. The activated cells were analyzed using Raman microspectroscopy as well as by other established biological methods to establish a correlation between spectral changes and molecular changes within the HSCs.

2 Materials and Method

2.1 *Cell Sample Preparation*

HSCs were isolated from 1-yr-old male Wistar rats. Livers were isolated and perfused under pentobarbital anesthesia (30 mg/kg), with Ca^{2+} and Mg^{2+} free Hanks' balanced salt solution (HBSS) for 10 min and then with Hanks containing 0.1% pronase E (Roche Diagnostics, Penzberg, Germany) for 15 min and with Hanks containing 0.04% collagenase (GIBCO-BRL, Burlington, Ontario) for another 15 min. Livers were minced and incubated at 37° C with constant shaking for 15 min in Dulbeco's modified eagle medium (DMEM) containing 0.01% DNase I. Hepatocytes were removed by centrifuging at 50 g for 4 min. HSCs were then isolated using Nycodenz (Axis-Shield PoC AS, Norway) density gradient centrifugation. To improve the purity of stellate cells, a third layer of 8% Nycodenz was added between 11% Nycodenz and DMEM layers as described by Oinonen et al.[18] After centrifugation, HSCs were collected from the 8% Nycodenz-DMEM interphase. Freshly isolated HSCs were plated on uncoated plastic tissue culture plates to induce HSCs *in vitro* activation at a density of $1.5\times10^5/cm^2$ in DMEM containing 10% calf serum. HSCs were identified by their typical microscopical appearance with characteristic retinoid droplets, autofluorescence emission, and immunochemical staining for desmin. The freshly isolated and the 4th, 8th, and 12th day cells in culture were examined by confocal Raman spectroscopy (CRS), and immunochemical staining for α-SMA (α-smooth muscle action).

HSCs were digested by 2.5 g/L trypsin and washed twice with phosphate-buffered saline (PBS) (pH 7.4). The HSC suspensions were diluted to an optical density of ~3.0. These suspensions were dropped on carriers of gold sheet for Raman detection and discarded after use.[19,20]

2.2 *Laser Confocal Microscopy*

To observe typical HSC microscopic appearance with characteristic retinoid droplets, a photograph of the freshly isolated HSCs were taken by a Nikon microscope camera FX-35WA connected to the inverted microscope (Nikon diaphot, Japan). Freshly isolated HSCs were also examined by laser confocal microscopy (Leica TCS SP2 MP, Germany) with a 328 nm excitation beam to identify the emission of blue/green autofluorescence in cells.

2.3 *Immunochemical Staining for Desmin*

The freshly isolated HSCs were smeared to the slides and fixed with acetone to perform immunochemical staining for desmin. The slides were incubated with 0.1% Triton-X 100 for 30 min, and then with 3% H_2O_2 for 10 min, and with 5% bovine serum albumin for another 30 min at 37°C. Then, the slides were incubated with the mouse monoclonal antibodies against desmin (Zymed, San Francisco, California; dilution 1:100) for 3 h at 37°C. Immunoreactivity was detected with the streptavidin-biotin-complex/immunoperoxidase (SABC) kit (Wuhan Boster Biological Technology Ltd., China) as the protocol. The sections were developed with 3,3′-diaminobenzidine tetrahydrochloride (Sigma, St. Louis, MO), and counterstained with haematoxylin. Replacement of the primary antibody with phosphate buffer solution (PBS) served as a negative control. Light microscopic examinations were made at 200 magnifications.

2.4 *Immunocytochemical Analysis for α-SMA of HSCs During Cultivation*

The freshly isolated and the 4th, 8th, and 12th day cultured cells were examined by immunochemical staining for α-SMA. Cell crawl slides were washed in PBS and fixed with acetone. Then, immunochemical staining was performed as already described except that the primary antibody was mouse anti-α-SMA monoclonal antibody (1:100; Wuhan Boster Biological Technology Ltd., China). Light microscopic examinations were made at 400×.

2.5 *Liver Tissue Sample Preparation*

The model animals used were 48 adult male Wistar rats (weighing 200 to 250 g). They were injected intraperitoneally with CCl_4 (2 mL/kg by weight) dissolved in olive oil. Eight rats were executed each time at the indicated time points: 4th, 12th, 24th, 32nd, 48th, and 64th h. Excision specimens taken from each rat were divided into two parts, one was used for immunohistological analysis, and the other was snap-frozen in liquid nitrogen and stored at −80°C until use. Cryosections (25 μm thick) were placed on a gold sheet for Raman detection. During the measurement, the liver tissue section was thawed to reach room temperature in air.

2.6 *Raman Spectroscopy*

A Renishaw Raman microspectrometer (System RM1000, Renishaw, Wotton under Edge, UK), similar to the system used by Maquelin et al.[21] was optimized for maximum throughput, detection sensitivity, and fluorescence suppression. The argon ion laser (Spectra Physics, Mountain View, California) provided a 20 mW excitation light at 514.5 nm. After attenuation through prisms and filters, the power of the laser exposed on the samples was only about 4 mW, which makes it almost impossible for the laser to lead to degradation of the tissues. Spectra were measured from tissues with a 20× short-working-distance objective [numerical aperture (NA) 0.40], and the signal was integrated for 30 to 60 s and measured over a spectral range of 600 to 1800 cm^{-1} with respect to the excitation frequency. The system included a stigmatic spectrometer with two motorized gratings, of which the 1800 grooves/mm grating was used to provide a spectral resolution of about 5 cm^{-1}. Raman scattering was detected by using an air-cooled 578×385 pixels CCD camera. Peak frequencies and rapid checking of instrumental performance were calibrated with the silicon phonon line at 520 cm^{-1}.

Spectra were recorded and processed (for smoothing, baseline subtraction, and peak detection) by means of the Grams/32 software (Thermo Galactic). Profile data were then imported into Origin 7.0 software (Origin Lab Corporation).

To minimize the autofluorescence of tissues under visible excitation, the CRS should be optimized by reducing the slit and CCD area to suppress fluorescence and achieve a better performance. Furthermore, laser bleaching was often employed, which means most samples should be irradiated by laser about 1 min to minimize its autofluorescence. This system had the highest spatial and spectral resolution; the laser was focused on a small spot within the sample. Theoretically, the size of laser spot in our experiments could be given by $s=0.61/\lambda/\mathrm{NA}$, and it was about 0.8 μm. The laser beam was focused manually on individual spots by means of a microscope objective to a spot of 1 to 2 μm in diameter. The power density was generally defined as the ratio of the power of the laser to the area of the spot, which means power density here was about 1 mw/μm^2. No differences were observed using 4-mW excitation laser between spectra collected for the same spot within consecutive 15 min duration focuses. Therefore, the spectra that were collected with such low excitation powers did not reveal changes that could be attributed to tissue heating.[22]

2.7 *Immunohistological Analysis for α-SMA in Liver Tissues*

A small sample of liver at the indicated time points was fixed in 10% buffered formalin and processed in paraffin wax. The 4 μm liver sections were deparaffinized and immunochemical staining was performed. The dewaxed formalin fixed sections were subjected to microwave heat antigen retrieval in citrate buffer 0.01 M, pH 6.0, for 5 min (80 to 90°C). The following steps were the same as immunochemical staining for α-SMA except that the incubation time of primary antibody was 2 h. Light microscopic examinations were made at 400× magnification.

2.8 *Autoclassifying System Based on Flow Cytometry and an Artificial Neural Network*

This software system, integrating the high robustness of an artificial neural network (ANN) and the strong quantity estimation ability of flow cytometry (FCM), was designed in our group previously.[23] It identifies regions of the sample that have similar spectral response by clustering the spectra into groups or clusters such that differences in the intracluster spectral responses are minimized while simultaneously maximizing the intercluster differences between spectral responses. To design neural network architecture, we must know how many clusters there are in the sample set. Also, a proper initial value of cluster centers to guarantee the convergence of algorithm should be available when FCM algorithm is used to classify. Supposing we do not know how many clusters there should be for a given set of data, a subtractive clustering method is a suitable one-pass algorithm for estimating the number and the value of cluster centers in a set of data. In the subtractive clustering algorithm, the number of clusters is increased gradually until the criterion to stop adding new clusters is reached.

3 Results

3.1 *HSC Identification*

After isolation of the HSCs, identification was performed by several methods. Phase-contrast microscopy of the freshly isolated cells demonstrated that HSCs appeared as small, dark cells with a granular cytoplasm [Fig. 1(a)]. In Fig. 1(b), the characteristic quick-fading autofluorescence (blue/green fluorescence) of retinoid droplets were observed in cells by fluorescence microscopy. By immunochemical staining, the freshly isolated cells were identified as desminpositive HSCs (brown yellow in cytoplasm) [Fig. 1(c)].

3.2 *HSC and Liver Tissue Raman Spectra*

The CRS technique yielded a rapid acquisition of high SNR (signal-noise-ratio) Raman spectra of the liver tissues and HSCs using 514.5 nm laser irradiation. Figure 2(a) shows average Raman spectra of the freshly isolated, 4th, 8th, and 12th day HSCs cultured on plastic. The frequencies of the Raman bands and some tentative assignments are given in Table 1. The Raman bands of HSCs, including the quiescent and activated HSCs, resulted primarily from protein and retinoid, such as amide I at 1660 cm^{-1}; amide III in the 1250 to 1300 cm^{-1} region; CH_2 (or CH_3) deformation vibration of protein at ~1450 cm^{-1}, C—C stretch (backbone) vibration of proteins at 1130, 1065, and 933 cm^{-1}; and CH_2 twisting and wagging vibration at 1340 cm^{-1}. Furthermore, there were more specific Raman bands for smaller molecular compounds, such as the very characteristic sharp band for ring-breathing vibration of phenylalanine at ~1006 and 960 cm^{-1}, which appeared in all protein-containing samples. Figure 2(b) shows the average Raman spectra of the eighth day HSCs (about 980 to 920 cm^{-1}), including the original (bottom) and subsequent second derivative spectrum (top). The band at 933 cm^{-1} can be seen with difficulty, due to overlapping of the vibration of phenylalanine, but definitely appears in its second-derivative spectrum. On the other hand, vibrational modes of retinoid also appeared in the spectra of two types of cells and showed obvious decrease accompanying the HSCs activation, such as the band at ~1587 cm^{-1}, which can be assigned to C═C stretching vibration of retinoid, and the band at 1364 and 1314 cm^{-1}, which may be assigned to CH_3 symmetrical deformation and HC═ in-plane deformation vibration of retinoid, respectively.

Figure 3 shows a series of average Raman spectra obtained from normal and injured rat liver tissues sections at the indicated time points including 4, 12, 24, 32, 48, and 64 h after CCl_4 injection. The primary Raman bands of tissues were observed at 1660, 1640, 1587, 1450, 1400, 1364, 1340, 1314, 1174, 1127, and 1006 cm^{-1}. There were nearly no macroscopic differences among these spectra except for bands at 1660 and 1640 cm^{-1}, which should be assigned[12] to vibration of amide I. This is described in detail in the following part.

3.3 *Immunochemical Staining for α-SMA*

The immunochemical staining (see Fig. 4) result of α-SMA (the marker of HSC activation) *in vitro* cultured HSCs showed that there were no expressions for the freshly isolated HSCs [Fig. 4(a)] and gradually increased during culture [brown yellow in cytoplasm seen in Figs. 4(b)–4(d)]. For liver tissues

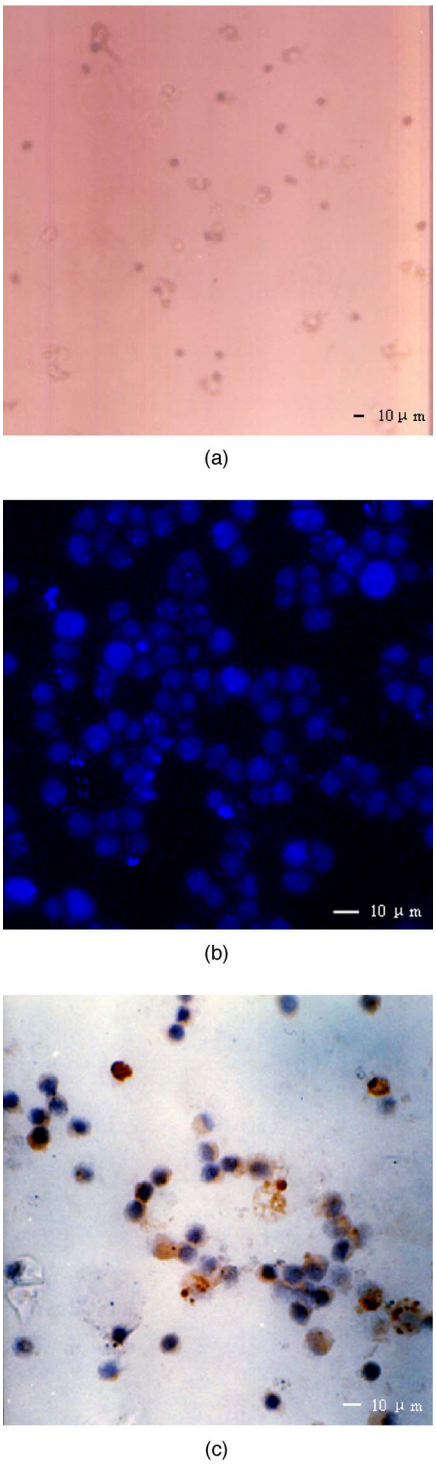

Fig. 1 Identification of the isolated HSCs: (a) photograph of the adhered HSCs taken by phase-contrast microscopy (×100); (b) photograph of the freshly isolated HSCs taken by laser confocal microscopy (×863); and (c) light microscopic appearance of the freshly isolated HSCs after staining for desmin (×200).

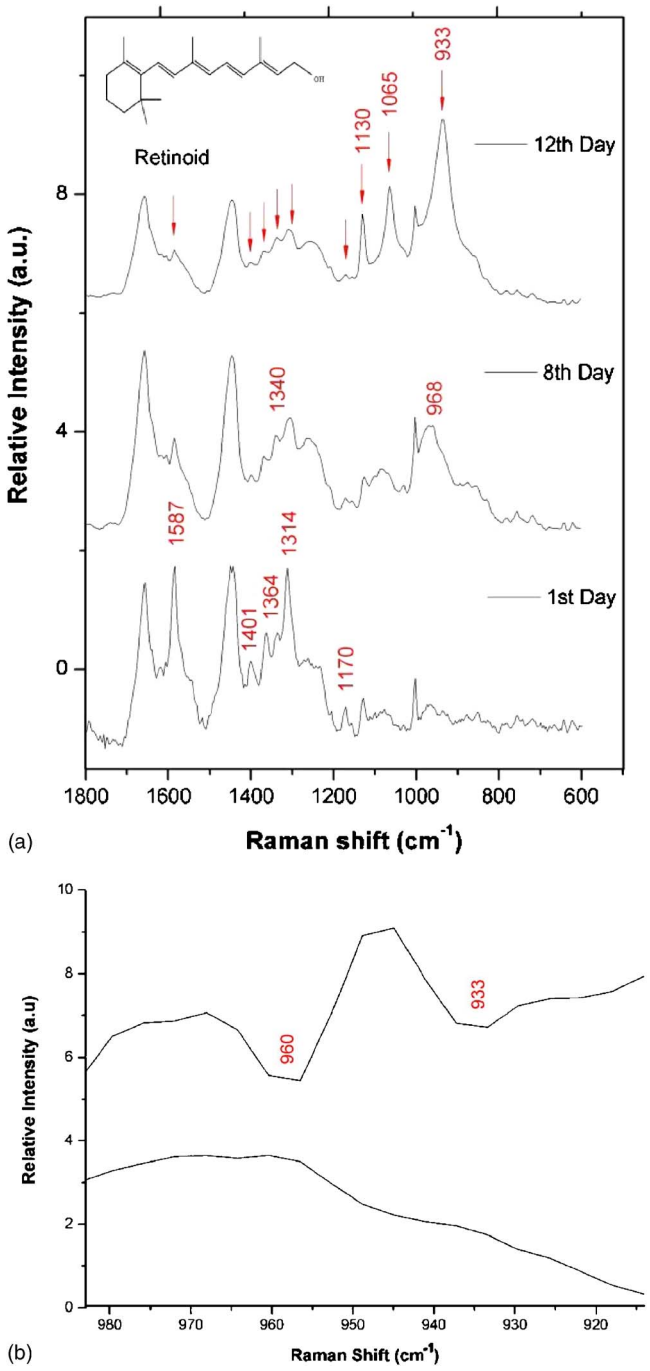

Fig. 2 (a) Average Raman spectra of the freshly isolated, 4th, 8th, and 12th day HSCs cultured on plastic, where the inset shows the molecular formula of retinoid, and (b) average Raman spectra of the eighth day HSCs (980 to 920 cm^{-1}), with the original spectrum at the bottom and the subsequent second-derivative spectrum at the top.

sections, the area and extent of α-SMA positive expression showed a maximal increase at the 32nd h from the 4th h after CCl_4 injection and gradually decreases after the 32nd h. The maximum of fatty infiltration, hepatocellular necrosis and the highest degree of lysosomal damage developed also at the 32nd hour, seen in Fig. 5(d), in which there were nearly no intact hepatocytes could be observed.

3.4 *Data Processing*

Since the same chemical bond always presents different Raman bands in different chemical circumstances, only the relative intensity of the respective Raman band is a reasonable

Table 1 Raman bands position and tentative assignments of quiescent and activated HSCs.

Raman Band Position (cm^{-1})	Assignments (Refs. 12, 14, 19, and 24)
1660	Protein, amide I
1587	Retinoid, C═C stretch
1440/1450	Lipid/protein, CH_2 def.
1401, 1170	Protein, hemoglobin
1364	Retinoid, CH_3 symmetrical def.
1340	Protein, CH_2 twist
1314	Retinoid, HC═ in-plane def.
1250–1300	Protein, amide III
1130, 1065, 933	Protein, C—C stretch (bk)
1006, 960	Protein, Phe

Abbreviations: bk; backbone; def., deformation; Phe, phenylalanine

index. Generally, the Raman band with highest intensity can be selected as an internal standard. In our study, the Raman band at 1587 cm^{-1} that should be assigned to retinol is the best choice used for normalization. The spectra of HSCs or liver tissues were obtained directly after laser exposure, and reveal a broad, featureless, and strong fluorescence background of specimens with 11 superimposed sharp Raman peaks. Normalized relative intensity of peak values of 11 Raman bands (~1660, ~1640, ~1587, ~1450, ~1400, ~1364, ~1340, ~1314, ~1174, ~1127, and ~1006 cm^{-1}) were used as the first 11 elements of feature vector $\boldsymbol{X}(x_1, x_2, x_3, \ldots, x_n,\ n=12)$. In addition to 11 normalized intensity of these Raman bands, one important relative intensity value of Raman shift were supplemented into our feature vector according to the elucidation mentioned above: I_{1640}/I_{1660} (amide I vibration of collagen). Raman spectra from 48 rat liver tissues of different injury degree were used to build and train our autoclassifying system. The six cluster center features are presented in Fig. 6. All the spectra of liver tissues were divided into six clusters corresponding to six time points, respectively.

4 Discussion

4.1 *In Vitro Activation of HSCs: Loss of Retinoid, Decrease of Hemoglobin, but Increase of α-Helical Protein*

From Fig. 2(a), note that the relative intensity of band at 1587 cm^{-1} in the freshly isolated HSCs became weaker step by step with the process of HSC *in vitro* activation. The band at 1587 cm^{-1} may be attributed to C═C stretching vibration of retinoid [the inset in Fig. 2(b) showed its molecular formula] according to related study in which Failloux et al.[24] demonstrated that the wavenumber of the more symmetrical C═C stretching mode ($\nu_{C=C}$) of retinol and all detected photoproducts, were expected to fall between 1500 and 1650 cm^{-1}. Retinoid (vitamin A), a primary alcohol consisting of a β-ionone core and a conjugated polyene chain (see the inset in Fig. 2), is important in many essential biological processes, including vision, glycoprotein synthesis, and reproduction, immunology, and cell growth.[25] The other two bands at 1364 and 1314 cm^{-1} in the spectra, which should be attributed to CH_3 symmetrical deformation vibration and HC═

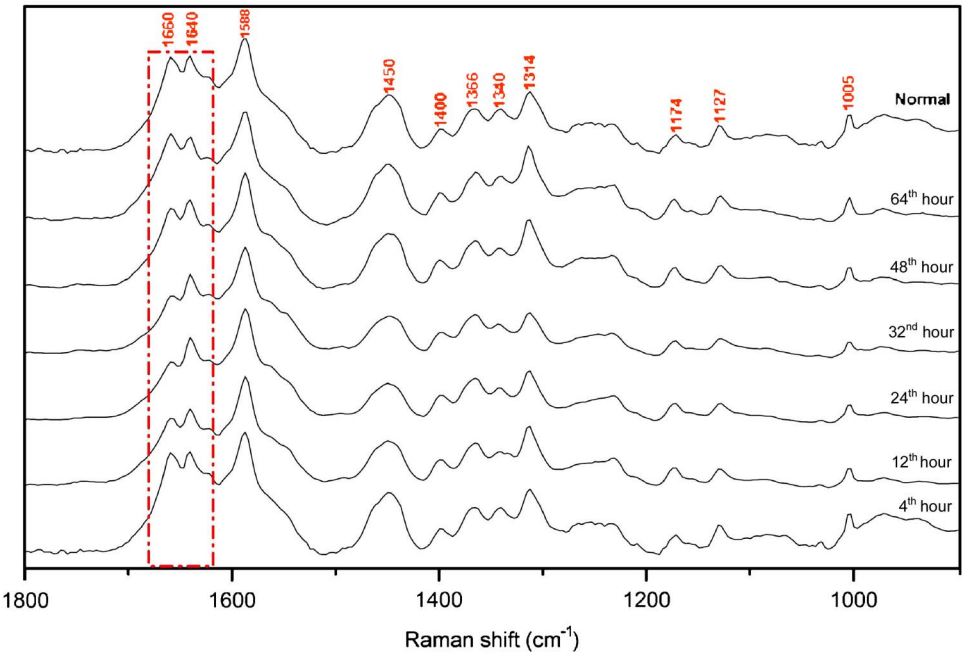

Fig. 3 Series of average Raman spectrums obtained from normal and injured rat liver tissue section on six time points after CCl_4 injection. From bottom to top: 4, 12, 24, 32, 48, and 64 h and normal.

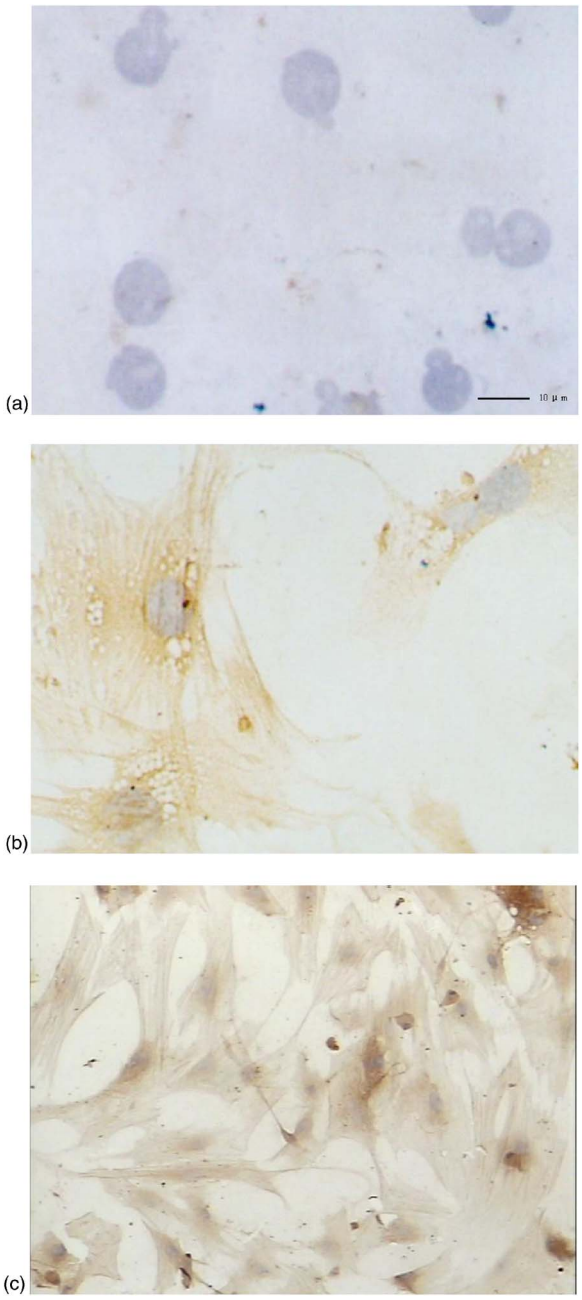

Fig. 4 Immunostaining for α-SMA of the (a) freshly isolated and (b) 4th, (c) 8th, and (d) 12th day HSCs in culture (×400). Positive staining of cells was observed in a fibrillar pattern in the cytoplasm.

in-plane deformation vibration, also confirmed that the band at 1587 cm^{-1} should be surely attributed to C═C stretching mode of retinoid.

Generally, the liver is a major organ of retinoid metabolism and storage, and more than 80% of the liver retinoid is stored in HSCs. Photographs of phase-contrast microscopy and fluorescence microscopy are shown in Fig. 1. It is obvious that lipid droplets existed in the freshly isolated HSCs. Other methods, such as transmission electronic microscopy (TEM), can also be used to observe the retinoid droplets with different size in the cytoplasm of quiescent[4] HSC. According to the already mentioned assignment of Raman bands, the consistent decreases associated with these three bands (1587, 1364, and 1314 cm^{-1}) undoubtedly proved that HSC *in vitro* activation resulted in the significant loss of retinoid droplets. Now the question arises about the metabolite of retinoid during the process of HSC activation. Okuno et al. presumed that the increased 9, 13-di-*cis*-retinoic acid (one of retinoid metabolites) in fibrotic liver may have a potential link between retinoid loss and transforming growth factor (TGF)-β mediated fibrogenesis *in vivo*.[26] However, no significant increase of this product, whose characteristic Raman band should appear in the region of 1500 to 1650 cm^{-1}, was observed in our study.

In addition, there were three Raman bands at 1130, 1065, and 933 cm^{-1} were obvious. These bands were all related to the modes of the C—C stretch vibration in protein.[12,27] Especially, the band at 933 cm^{-1} is usually used to characterize the secondary structure of protein and here should be assigned to the C—C stretching vibration of α-helical protein. Generally, Raman spectroscopy has proved to be a very sensitive technique characterizing the secondary structure of protein.[12] Here, we question how to understand the obvious increase for the relative intensity of band at 933 cm^{-1}. It is well known that *in vitro* activation of HSCs associated with overexpression of α-SMA, and α-SMA is a kind of cytoskeleton and also an α-helical protein; its accumulation for HSC activation may be the main reason[12,27] of the intensity increase of Raman band at 933 cm^{-1}. As shown in Fig. 2(a), the 12th HSCs displayed increased intensity at 933 cm^{-1}, which indicates a greater content of the protein with α-helix structure known to exist in activated HSCs, because they contain α-SMA rather than quiescent ones. Due to overlapping of the vibrations of phenylalanine, the spectral profile with a signal attributable to the Raman band at 933 cm^{-1} $(C—C)_{\alpha}$ was difficult to be observed, but definitely appeared in its second-derivative spectrum for the 8th day HSCs [shown in Fig. 2(b)]. This suggested the protein with α-helix structure (α-SMA) could be detected when its content increased gradually along with *in vitro* HSC activation. If the period of *in vitro* HSC activation was divided into early, middle, and later stages, the 8th and 12th days should correspond to middle and later stages, respectively. When the phenotype of HSCs was changing into myofibroblast-like cells (namely, in the 12th day HSCs) completely, CRS could sensitively characterize their rapid molecular changes. Accordingly, the result of α-SMA immunocytochemistry analysis also (see Fig. 4) showed that there is no expression for the freshly isolated HSCs but distinct expression for the 12th day HSCs, which confirm our results of Raman detection.

4.2 *In Vivo Activation of HSCs: The Increase of Collagen in Liver Tissues*

As shown in Fig. 3, the ratio of the relative intensity of bands at 1640 and 1660 cm^{-1} showed regular changes from the bottom to top of the spectrum. In detail, this ratio, namely, I_{1640}/I_{1660} starting from hour 4 gradually increased until hour 32 and subsequently decreased step-by-step by hour 64. The top profile represented the Raman spectrum of normal liver tissue and looked the same with that of the 64 h injured tissue, which indicated that rat liver had been recovered from the injury state completely. It was determined that Raman band at 1640 cm^{-1} should be assigned to a characteristic vi-

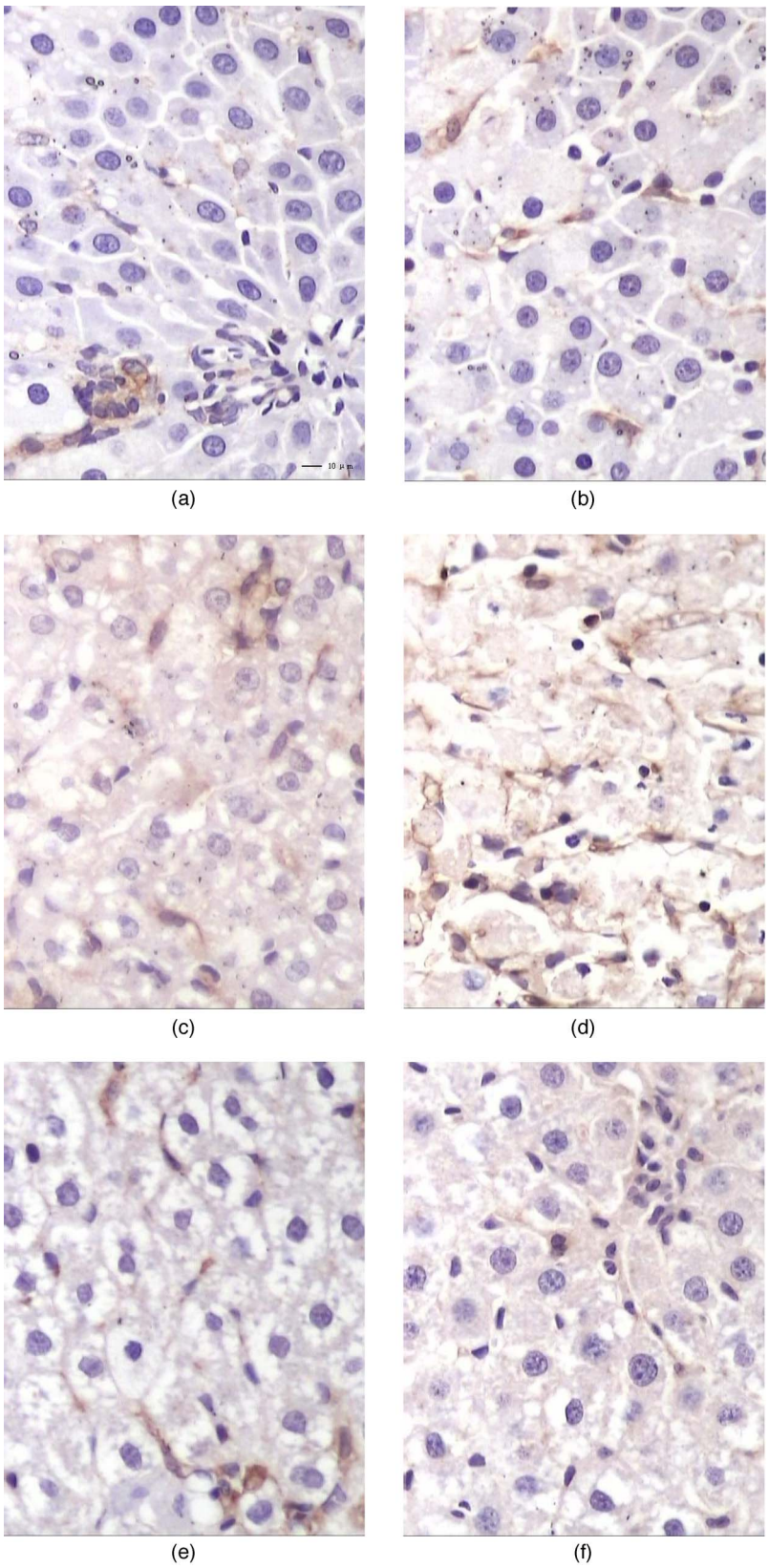

Fig. 5 Immunostaining for α-SMA of liver tissues section at the indicated time points: (a) 4, (b) 12, (c) 24, (d) 32, (e) 48, and (f) 64 h (×400).

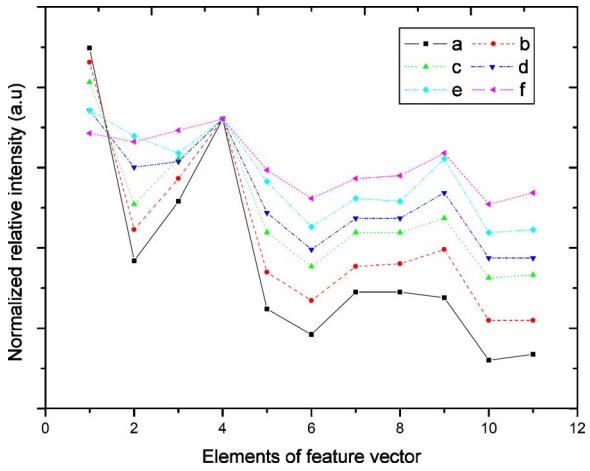

Fig. 6 Profile of six cluster centers of normalized relative intensity.

bration mode of collagen.[12] Why did the content of collagen show a maximal increase at hour 32 in this case? What was the relationship among rat liver injury, increased collagen, and even HSCs *in vivo* activation? Lee et al. identified HSC proliferation and showed a maximal increase at hour 32 after CCl_4 injection,[5] and our immunohistogical study (Fig. 5) also showed a positive increase for α-SMA and maximal degree of hepatocytes injury at hour 32 after CCl_4 injection. These suggested HSC *in vivo* activation and the degree of liver injury achieve to a peak about at hour 32 after a single injection of CCl_4. The major function of activated HSCs in liver injury was to secrete extracellular matrix (ECM) containing fibril-forming collagens. Therefore, the ratio of a characteristic vibration mode of collagen may be regarded as the extent of HSC activation *in vivo* and the degree of liver injury.

4.3 *Spectral Clustering Analysis of Liver Tissues Using the Autoclassifying System*

Raman spectroscopy is an efficient technique applied to characterization of HSCs, but an important aspect that should not be underestimated is that the type of information obtained through Raman spectroscopy may be new to hepatologists. In addition, Raman spectroscopy will potentially be utilized to study the HSC activation *in vivo* in the near future, and it is urgent determine a way to automatically accomplish the judgment of HSC activation.

According to empiric and some criteria a conclusion can be safely drawn that cluster in Fig. 6(a) has the highest probability to be a 32nd hour tissue and the cluster in Figs. 6(e) and 6(f) has the highest probability to be normal tissue (see Fig. 6). It can be easily determined that the cluster in Fig. 6(a) has a high intensity at 1640 cm^{-1}, and this band is always assigned to amide I stretching of collagen and represents more collagen in the liver tissue as result of HSC *in vivo* activation, which is a distinct sign of HSC *in vivo* activation.

Another set of 20 samples was used to test our classifying system. The result is almost the same as the result classified by hand, and only two spectral data conflict with the result of hand classifying, which means a 90% accuracy rate. Considering the relatively small initial training set, this result is satisfactory. Also compared with accuracy rates of 85 and 75% for the FCM method alone and the ANN method alone, respectively, the combination of FCM and ANN is recommended. To achieve improvement and facilitate the perspective application in clinic application, future work will focus on building an expert knowledge database for proper choice of feature vector and optimizing the design of ANN structure and clustering method.

5 Conclusions

This paper demonstrated the application of Raman spectroscopy to study HSCs and obtain satisfactory results consistent with other methods. The spectroscopic results revealed that Raman analysis of single isolated HSC cultured on plastic and CCl_4 induced injury rat liver tissue provide a novel, rapid, reagent free, and nondestructive technique for study of HSCs *in vitro* and *in vivo* activation. A tentative user-friendly autoclassifying system was applied to classify Raman spectra of rat liver tissues and provided more credible classifying results for automatically evaluating the degree of HSC *in vivo* activation. Liver fibrosis is reversible, whereas cirrhosis, the end-stage consequence of fibrosis, is generally irreversible. Thus, efforts to slow the progression of fibrosis focus primarily on events that lead to the early accumulation of scarring, in hopes of identifying its molecular changes. A liver biopsy analyzed with connective tissue stains has long been considered the "gold standard" for assessing liver histology, disease activity, and liver fibrosis. However, biopsy is associated with potential morbidity and mortality, and has several limitations.[28] Raman spectroscopy in conjunction with a fiber optic probe can potentially accomplish *in vivo*, *in situ* monitoring for the molecular changes of the early accumulation of scarrings, and further whether the liver fibrosis is reversible or has evolved to liver cirrhosis. Accordingly, this technique shows considerable promise as an accurate diagnostic test for early liver fibrosis clinically, and we think it will be of interest for a wide range of scientists in this field.

Acknowledgments

The authors gratefully acknowledge all the staff of Institute of Analytical Biomedicine (IAB), Wuhan University, for their generous cooperation. This project was supported by the National Natural Science Foundation of China under Grants 20405011, 90409013, 30371666, and 20375029.

References

1. A. Reuben, "Ito becomes a star," *Hepatology (Philadelphia, PA, U.S.)* **35**, 503–504 (2002).
2. R. Blomhoff, M. H. Green, J. B. Green, T. Berg, and K. R. Norum, "Vitamin A metabolism: new perspectives on absorption, transport, and storage," *Physiol. Rev.* **71**, 951–990 (1992).
3. S. L. Friedman, "Molecular regulation of hepatic fibrosis, an integrated cellular response to tissue injury," *J. Biol. Chem.* **275**, 2247–2250 (2003).
4. T. Wu and G. J. Teng, "Culture and identification of the rat hepatic stellate cells," *Mod. Med. J.* **32**, 303–306 (2004).
5. J. I. Lee, K. S. Lee, Y. H. Paik, Y. N. Park, K. H. Han, C. Y. Chon, and Y. M. Moon, "Apoptosis of hepatic stellate cells in carbon tetrachloride induced acute liver injury of the rat: analysis of isolated hepatic stellate cells," *J. Hepatol* **39**, 960–966 (2003).
6. R. Whalen, D. C. Rockey, S. L. Friedman, and T. D. Boyerl, "Activation of rat hepatic stellate cells leads to loss of glutathione s-transferases and their enzymatic activity against products of

oxidative stress," *Hepatology (Philadelphia, PA, U.S.)* **30**, 927–933 (1999).
7. S. Vogel, R. Piantedosi, J. Frank, A. Lalazar, D. C. Rockey, S. L. Friedman, and W. S. Blaner, "An immortalized rat liver stellate cell line (HSC-T6): a new cell model for the study of retinoid metabolism *in vitro*," *J. Retin. Res.* **41**, 882–893 (2000).
8. G. J. Puppels, F. F. de Mul, C. Otto, J. Greve, M. Robert-Nicoud, D. J. Arndt-Jovin, and T. M. Jovin, "Studying single living cells and chromosomes by confocal Raman microspectroscopy," *Nature (London)* **347**, 301–303 (1990).
9. I. Notingher, S. Verrier, S. Haque, J. M. Polak, and L. L. Hench, "Spectroscopic study of human lung epithelial cells (A549) in culture: living cells versus dead cells," *Biopolymers* **72**, 230–240 (2003).
10. I. Notingher, G. Jell, U. Lohbauer, V. Salih, and L. L. Hench, "In situ non-invasive spectral discrimination between bone cell phenotypes used in tissue engineering," *J. Cell. Biochem.* **92**, 1180–1192 (2004).
11. G. Deinum, D. Rodriguez, T. J. Römer, M. Fitzmaurice, J. R. Kramer, and M. S. Feld, "Histological classification of Raman spectra of human coronary artery atherosclerosis using principal component analysis," *Appl. Spectrosc.* **53**, 938–942 (1999).
12. A. Mahadevan-Jansen and R. Richards-Kortum, "Raman spectroscopy for the detection of cancers and precancers," *J. Biomed. Opt.* **1**, 31–70 (1996).
13. C. D. Sudworth and N. Krasnera, "Raman spectroscopy of Alzheimer's diseased tissue," *Proc. SPIE* **5321**, 93–101 (2004).
14. A. G. Shen, Y. Ye, X. H. Wang, C. C. Chen, H. B. Zhang, and J. M. Hu, "Raman scattering properties of human pterygium tissue," *J. Biomed. Opt.* **10**, 024036 (2005).
15. P. Rösch, M. Harz, M. Schmitt, and J. Popp, "Raman spectroscopic identification of single yeast cells," *J. Raman Spectrosc.* **36**, 377–379 (2005).
16. P. J. Caspers, A. C. Williams, E. A. Carter, H. G. M. Edwards, B. W. Barry, H. A. Bruining, and G. J. Puppels, "Monitoring the penetration enhancer dimethyl sulfoxide in human stratum corneum *in vivo* by confocal Raman spectroscopy," *Pharm. Res.* **19**, 1577–1580 (2002).
17. S. R. Hawi, W. B. Campbell, A. Kajdacsy-Balla, R. Murphy, F. Adar, and K. Nithipatikom, "Characterization of normal and malignant human hepatocytes by Raman microspectroscopy," *Cancer Lett.* **110**, 35–40 (1996).
18. T. Oinonen, T. Koivisto, and K. O. Lindros, "No significant expression of CYP2E1 in rat liver stellate cells," *Biochem. Pharmacol.* **15**, 1075–1107 (1998).
19. A. G. Shen, Y. Ye, J. W. Zhang, X. H. Wang, J. M. Hu, W. Xie, and J. Shen, "Screening of gastric carcinoma cells in the human malignant gastric mucosa by confocal Raman microspectroscopy," *Vib. Spectrosc.* **37**, 225–231 (2005).
20. K. C. Schuster, I. Reese, E. Urlaub, J. R. Gapes, and B. Lendl, "Multidimensional information on the chemical composition of single bacterial cells by confocal Raman microspectroscopy," *Anal. Chem.* **72**, 5529–5534 (2000).
21. K. Maquelin, L. P. Choo-Smith, T. van Vreeswijk, H. P. Endtz, B. Smith, R. Bennett, H. A. Bruining, and G. J. Puppels, "Raman spectroscopic method for identification of clinically relevant microorganisms growing on solid culture medium," *Anal. Chem.* **72**, 12–19 (2000).
22. M. G. Shim and B. C. Wilson, "The effect of ex vivo handling procedures on the near-infrared Raman spectra of normal mammalian tissues," *Photochem. Photobiol.* **63**, 662–671 (1996).
23. Y. Y. Tan, A. G. Shen, J. W. Zhang, N. Wu, L. Feng, Q. F. Wu, Y. Ye, and J. M. Hu, "Design of auto-classifying system and its application in Raman spectroscopy diagnosis of gastric carcinoma," in *Proc. Int. Conf. Mach. Learn. Cybern.* Vol. **3**, pp. 1360–1363 (2003).
24. N. Failloux, I. Bonnet, E. Perrier, and M. H. Baron, "Effects of light, oxygen and concentration on vitamin A1," *J. Raman Spectrosc.* **35**, 140–147 (2004).
25. M. J. O'Connell, R. Chua, B. Hoyos, J. Buck, Y. Chen, F. Derguini, and U. Hämmerling, "Retro-retinoids in regulated cell growth and death," *J. Exp. Med.* **184**, 549–555 (1996).
26. M. Okuno, T. Sato, T. Kitamoto, S. Imai, N. Kawada, Y. Suzuki, H. Yoshimura, H. Moriwaki, K. Onuki, S. Masushige, Y. Muto, S. L. Friedman, S. Kato, and S. Kojima, "Increased 9,13-di-cis-retinoic acid in rat hepatic fibrosis: implication for a potential link between retinoid loss and TGF-beta mediated fibrogenesis *in vivo*," *Hepatology (Philadelphia, PA, U. S.)* **30**, 1073–1080 (1999).
27. C. Kraffta, T. Knetschke, A. Siegner, R. H. W. Funk, and R. Salzer, "Mapping of single cells by near infrared Raman microspectroscopy," *Vib. Spectrosc.* **32**, 75–83 (2003).
28. S. L. Friedman, "Liver fibrosis—from bench to bedside," *Hepatology (Philadelphia, PA, U. S.)* **38**, S38–S53 (2003).